Neurobiology of Disease 210 (2025) 106919

Contents lists available at ScienceDirect

Neurobiology of Disease

journal homepage: www.elsevier.com/locate/ynbdi

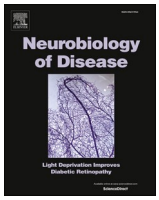

Circulating myeloid-derived suppressor cell load and disease severity are associated to an enhanced oligodendroglial production in a murine model of multiple sclerosis

Mari Paz Serrano-Regal [a,b,1,2], Celia Camacho-Toledano [a,b,c,1], Inmaculada Alonso-García [a,b], María Cristina Ortega [a,b,c], Isabel Machín-Díaz [a,b,c], Rafael Lebrón-Galán [a], Jénnifer García-Arocha [a], Leticia Calahorra [a,b], Manuel Nieto-Díaz [d,e], Diego Clemente [a,b,c,*]

[a] Neuroimmune-Repair Group, Hospital Nacional de Parapléjicos-SESCAM, Finca La Peraleda s/n, 45071 Toledo, Spain
[b] Neuroimmune-Repair Group, Instituto de Investigación Sanitaria de Castilla-La Mancha (IDISCAM). Spain
[c] Centro de Investigación Biomédica en Red de Enfermedades Neurodegenerativas (CIBERNED), Carlos III Health Institute, Avd. Monforte de Lemos, 3-5, 28029 Madrid, Spain
[d] Molecular Neuroprotection Group, Hospital Nacional de Parapléjicos-SESCAM, Finca La Peraleda s/n, 45071 Toledo, Spain
[e] Molecular Neuroprotection Group, Instituto de Investigación Sanitaria de Castilla-La Mancha (IDISCAM). Spain

ARTICLE INFO

Keywords:
Myelin
EAE
MDSCs
OPCs
Demyelination
Biomarkers

ABSTRACT

Multiple sclerosis (MS) is a highly heterogeneous immune-mediated demyelinating disease. Myelin restoration is essential to prevent disability progression in MS patients. However, remyelinating therapies are failing in clinical trials, in part, due to the lack of biomarkers that classify the differing endogenous regenerative capacities of enrolled patients. In the experimental autoimmune encephalomyelitis (EAE) MS model, circulating monocytic myeloid-derived suppressor cells (M-MDSCs) are associated to milder disease courses, better recovery and less degree of tissue damage. Here, we show that disease severity affects the gradient of oligodendrocyte precursor cells (OPCs) present in mixed active-inactive lesions of MS patients, along with a positive correlation between M-MDSC density and OPC abundance. EAE disease severity negatively influences the density of total and newly generated OPCs found associated to the demyelinated lesions. In addition, disease severity also impacts the abundance of newly generated oligodendrocytes throughout the EAE disease course. Interestingly, circulating M-MDSCs at EAE onset and peak of the disease are directly associated to a higher density of newly generated oligodendrocytes in the demyelinated lesions. Our results set the basis for further studies on M-MDSCs as a promising new biomarker that identify a CNS prone to new oligodendrocyte generation in response to an inflammatory insult.

Abbreviations: Arg-I, Arginase-I; cAIL, core of mixed active/inactive lesions; CFA, complete Freund's Adjuvant; CNS, central nervous system; DAB, 3, 3′-diaminobenzidine; DMT, disease modifying treatment; EAE, experimental autoimmune encephalomyelitis; EC, eriochrome cyanine; EDSS, Expanded Disability Status Scale; FBS, fetal bovine serum; HLA, human leukocyte antigen; HPF, high power field; IHC, immunohistochemistry; IQR, interquartile range; ip, intraperitoneal; mAILs, mixed active/inactive lesions; MDSCs, myeloid-derived suppressor cells; M-MDSCs, monocytic-myeloid-derived suppressor cells; MOG, myelin oligodendrocyte glycoprotein; MRI, magnetic resonance imaging; MS, multiple sclerosis; NAWM, normal appearing white matter; NDS, normal donkey serum; OLs, mature oligodendrocytes; OPC, oligodendrocyte precursor cell; P/S, Penicillin/Streptomycin; PB, 0.1 M Phosphate Buffer, pH 7.4; PBS, sterile 1× Phosphate Buffered Saline; PBST, 0.1 % Triton X-100 in PBS; PET, positron emission tomography; PFA, paraformaldehyde; rAILs, rim of mixed active/inactive lesions; RRMS, relapsing-remitting multiple sclerosis; RT, room temperature; SI, severity index; WM, adjacent white matter.

* Corresponding author at: Grupo de Neuroinmuno-Reparación, Hospital Nacional de Parapléjicos, Finca *"La Peraleda"* s/n, E-45071 Toledo, Spain.
E-mail address: dclemente@sescam.jccm.es (D. Clemente).

[1] Similar contribution of these authors

[2] Current address: Universidad Europea de Madrid. School of Medicine, Health and Sports. Department of Physiotherapy.

https://doi.org/10.1016/j.nbd.2025.106919
Received 12 February 2025; Received in revised form 14 April 2025; Accepted 16 April 2025
Available online 16 April 2025

1. Introduction

Multiple sclerosis (MS) is an immune-mediated disorder of the central nervous system (CNS) characterized by focal demyelination, gliosis and axonal degeneration, and represents the leading cause of non-traumatic disability among young adults (Filippi et al., 2018; Koch-Henriksen and Sørensen, 2010). The most common form of MS is relapsing-remitting MS (RRMS), which is characterized by episodes of neurological dysfunction (relapses) followed by periods of full or partial recovery (remission) (Dendrou et al., 2015). RRMS is highly heterogeneous in terms of disease course and symptoms (Correale et al., 2023) and the progression of MS appears to result from the interplay between acute inflammatory relapses, chronic inflammation in the CNS, the degeneration of axons and loss of oligodendrocytes. Increased resilience in both rates axon degeneration rates and remyelination efficiency during early stages of the disease has been proposed as the basis for the heterogeneous severity found in this clinical MS subtype (Kotelnikova et al., 2017).

In MS, axonal loss - and the subsequent neurodegeneration- is directly associated with the permanent functional deficits observed in patients, likely stemming from the vulnerability of denuded axons (Kornek et al., 2000). The loss of myelin can be repaired by the spontaneous generation of new myelin sheaths around the axons, *i.e.*, remyelination. Remyelination is associated with axonal preservation (Kornek et al., 2000) and reduced disability levels in MS patients (Bodini et al., 2016). However, its efficiency decreases significantly with age and disease progression (Franklin and Ffrench-Constant, 2017). In this regard, it has been hypothesized that impaired activation, recruitment and differentiation of oligodendrocyte precursor cell (OPC)are among the main putative causes of remyelination failure (Boyd et al., 2013; Kotter et al., 2006; Kuhlmann et al., 2008; Tepavčević et al., 2014). Therefore, improving OPC proliferation/recruitment to demyelinated areas as well as OPC differentiation, could suffice myelinating cells to accomplish effective remyelination and, lately, prevent neurodegeneration. Importantly, interindividual variability in the endogenous ability to induce these processes (OPC proliferation and differentiation) within the CNS of MS patients has not yet been thoroughly explored.

Currently, all available disease-modifying treatments (DMTs) for MS are immunomodulators and/or immunosuppressants that reduce disease activity and relapse frequency but do not efficiently prevent disability progression. Consequently, one of the key therapeutic challenges in MS is identifying molecules that enhance remyelination and promote neuroprotection, which in turn would stop or slow disease progression (Lubetzki et al., 2020). The lack of suitable biomarkers of regeneration coupled with the heterogeneous remyelination profiles observed among MS patients (Lubetzki et al., 2020) may partially explain why myelin repair molecules are failing in clinical trials. Therefore, the identification of new classifying biomarkers indicative of a CNS prone to efficiently induce OPC proliferation and differentiation would improve the success rate of clinical trials with pro-remyelinating molecules.

Experimental autoimmune encephalomyelitis (EAE), the most commonly used animal model of MS, has been extensively employed to study the pathogenesis of the disease as well as to carry out preclinical evaluation of candidate pro-remyelinating molecules (Cordano et al., 2022; Deshmukh et al., 2013; Ineichen et al., 2017; Lubetzki et al., 2020; Mei et al., 2016). Individualized evaluation of EAE represents an excellent strategy to find clinically translatable biomarkers of responsiveness and efficacy of DMTs (Camacho-Toledano et al., 2022). This approach has been used to study the interplay between disease severity and CNS-related histopathological events, as milder disease courses are associated with less demyelination and axonal damage (Melero-Jerez et al., 2020). However, the impact of the heterogeneous disease severity on the capacity of the CNS to produce new mature oligodendrocytes (OLs) after a neuroinflammatory insult remains elusive.

Monocytic myeloid-derived suppressor cells (M-MDSCs) are a heterogeneous population of regulatory cells of the innate immune response originating in the bone marrow. Under pathological conditions or inflammatory contexts, they remain undifferentiated and acquire immunosuppressive functions (Bronte et al., 2016). The presence and characterization of M-MDSCs in the spinal cord of EAE mice at the peak of the disease course have been previously described (Moliné-Velázquez et al., 2011). Interestingly, there is a direct association between the presence of M-MDSCs in the lesion and the presence of OPCs in the adjacent perilesion in spinal cord demyelinating areas of mice with EAE. Furthermore, M-MDSCs influence various aspects of OPC biology *in vitro* (survival, proliferation and differentiation) through the release of the soluble factor osteopontin (Melero-Jerez et al., 2021). Our group has pioneered the morphological identification of cells expressing all the bona-fide markers of M-MDSCs in *post-mortem* tissue from MS patients. Notably, there is a direct relation between the density of M-MDSCs in MS tissue and disease severity (Ortega et al., 2023). In the EAE model, circulating M-MDSCs at disease onset were associated with milder disease courses and less degree of demyelination and axonal damage in the spinal cord, while at peak were indicative of better symptom recovery (Ortega et al., 2023).These findings suggest that M-MDSCs are an excellent predictive biomarker of disease severity in the EAE model. However, little is known about whether the abundance of circulating M-MDSCs could predict an enhanced ability of the CNS to produce new OPCs able to differentiate into OLs.

In this work, we found a direct association between disease duration and the relative density of OPCs in mixed active/inactive lesions (mAIL) of MS patients. Moreover, the density of OPCs at the rim of these lesions (rAIL) directly correlated with the abundance of M-MDSCs present in the same areas. In addition, we demonstrate that milder courses of EAE are associated with a higher presence of proliferating OPCs at the end of the effector phase and of newly generated OLs at the end of the recovery phase, both located in the perilesion of demyelinated spinal cord areas. Notably, a higher content of circulating M-MDSCs at the onset or the peak of the disease is associated with a lesion and perilesion enriched in newly generated OLs, respectively, once each animal has reached its maximal clinical recovery. These results pave the way for the potential use of circulating M-MDSCs as a promising biomarker of a CNS more prone to produce new OLs in inflammatory conditions such as MS.

2. Material and methods

2.1. Human tissue and MS lesion classification

Post-mortem snap-frozen cortical tissue blocks containing mAIL from eight MS patients were analyzed (supplied by the UK MS Tissue Bank; Table 1). mAIL were classified based on demyelination and cellular distribution as previously described (Clemente et al., 2011; Kuhlmann et al., 2017; Luchetti et al., 2018): demyelinated areas with a hypocellular core (cAIL) surrounded by a rAIL enriched in human-leukocyte antigen (HLA)-DR positive cells. Moderate T cell infiltration was observed in the cAIL. Apart from sex and the clinical form of MS, disease duration was also considered for patient classification. Long disease duration was defined as disease course exceeding the median of the

Table 1
Demographic and clinical data of MS patients for the histopathological analysis.

Patient	MS	Age	Sex	TP (h)	DD (y)
MS94	PP	42	F	11	6
MS363	PP	42	M	20	27
MS383	PP	42	M	17	17
MS398	PP	57	F	28	28
MS356	SP	45	F	10	16
MS406	SP	62	M	23	47
MS408	SP	39	M	21	10
MS470	SP	64	F	nd	35

Abbreviations: DD, disease duration; F, female; h, hours; M, male; PP, primary-progressive; SP, secondary-progressive; TP, time *post-mortem*; y, years.

histopathological cohort [22 years, interquartile range (IQR), 13–31.5], whereas short disease duration referred to a clinical course of less than 22 years.

2.2. Immunohistochemistry and Eriochrome Cyanine for myelin staining in human tissue

Cryosections (10 μm thick, Leica) from MS tissue were air-dried for 45 min at room temperature (RT) and fixed in 4 % paraformaldehyde (PFA; Sigma Aldrich)in 0.1 M Phosphate Buffer, pH 7.4 (PB) for 1 h. Immunohistochemistry (IHC) for HLA-DR and OPCs was carried out by incubating with anti-human HLA-DR (1:200; Agilent, M0746, TAL.1B5 clone) and anti-human NG2 (1:25; clone 9.2.27, BD Bioscience) individually in parallel tissue slides. Detection of NG2 was visualized using the TSA signal amplification system (TSA Biotin Kit, AkoyaBio) followed by incubation with appropriate biotinylated secondary antibodies (1:200; Vector Labs). The IHC reaction was developed using the Vectastain Elite ABC reagent (Vector Labs) and the peroxidase reaction product was visualized with 0.05 % 3,3′-diaminobenzidine (DAB, Sigma-Aldrich) and 0.003 % H_2O_2 in 0.1 M Tris-HCl, pH 7.6. The reaction was monitored under the microscope and terminated by rinsing the slides with PB. After NG2 IHC, cell nuclei were counterstained with Agilent Giemsa Stain Kit (AR164, Artisan). To visualize myelin following HLA-DR IHC, Eriochrome Cyanine (EC) staining was carried out as described elsewhere (Ortega et al., 2023). In all cases, sections were dehydrated and mounted using Entellan mounting medium.

M-MDSCswere identified in parallel tissue slices from the same patients by immunofluorescence with a combination of three markers to distinguish these cells from other myeloid populations including neutrophils or inflammatory macrophages as described previously (Ortega et al., 2023): the monocytic marker CD14 (always expressed by M-MDSCs, 1:25, R&D, BAF383), the granulocytic protein CD15 (absent in M-MDSCsas it is typically expressed by mature neutrophils and the polymorphonuclear subset of MDSCs, 1:25, Agilent ISO62, carb3 clone) and the specific molecule of antigen presenting-cells HLA-DR (low or absent in M-MDSCs; 1:100, Agilent M076, TAL.1B5 clone). After incubating the tissue with the primary antibodies, the appropriate Alexa fluorescent-tagged secondary antibodies were used (1:1000, Invitrogen) and cell nuclei were stained with Hoechst 33342 (10 μg/mL, Sigma-Aldrich).

2.3. OPC and M-MDSC quantification in mAIL

By using HLA-DR IHQ and EC, rAIL was defined as the region between the border of the demyelinated core (cAIL) and the adjacent non-demyelinated white matter enriched with HLA-DR$^+$ cells. We also defined the adjacent normal-appearing white matter (NAWM) as the non-lesional white matter one high-power field (HPF) at 40× (0.0485 mm^2 per HPF) away from the end of the rAIL (Kessler et al., 2023). Only those mAILs where all 3 regions were clearly identified (cAIL, rAIL, and NAWM) were quantified. We randomly selected 5 HPF per region from the slide with NG2 immunostaining. Elements with Giemsa-positive nuclei surrounded by NG2 labelling were considered as OPC (NG2$^+$ cells). The density of OPCs/mm^2 in each region was calculated as the average number of NG2$^+$ cells per HPF (0.0485 mm^2). In addition, the ratio of the OPC density relative to each area (rAIL/cAIL, NAWM/rAIL, and NAWM/cAIL) was determined. HPF at 40× magnification of the three regions were captured using a BX61 microscope (Olympus) connected to an MBF CX9000 colour camera. M-MDSC density quantification in the rAIL was carried out as described previously(Ortega et al., 2023).

2.4. Induction of EAE

Chronic progressive EAE was induced in female 8-week-old C57BL/6 mice (Janvier Labs, France) by immunization with 200 μL of a Myelin Oligodendrocyte Glycoprotein (MOG) solution (200 μg, $MOG_{35–55}$ peptide: Genscript, New Jersey, USA) emulsified in complete Freund's Adjuvant (CFA) containing 4 mg/mL of heat-inactivated *Mycobacterium tuberculosis* (BD Biosciences, Franklin Lakes, New Jersey, USA). Immunized mice were administered Pertussis toxin intravenously through the tail vein (250 ng/mouse: Sigma-Aldrich, St. Louis, MO, USA) in a final volume of 100 μL on the day of immunization and 48 h later. EAE was scored clinically on a daily basis in a double-blind manner as follows: 0, no detectable signs of EAE; 0.5, half limp tail; 1, complete limp tail; 1.5, hind limb inhibition (unsteady gait and/or poor hind leg grip); 2, hind limb weakness; 2.5, bilateral partial hind limb paralysis or unilateral full hind limb paralysis; 3, complete bilateral hind limb paralysis (paraplegia); 3.5, partial forelimb paralysis; 4, tetraplegia; 4.5, moribund; and 5, death. In accordance with ethical regulations, humane end-point criteria were applied when an animal reached a clinical score $\geq$ 4, when clinical score $\geq$ 3 persisted for more than 48 h, or when self-mutilation was evident, persistent urine retention, 35 % weight loss, or signs of stress or pain for more than 48 h, even if the EAE score was <3. All animal manipulations were approved by the institutional ethical committee (*Comité Ético de Experimentación Animal del Hospital Nacional de Parapléjicos*), and all experiments were carried outin compliance with the European guidelines for animal research (European Council Directive 2010/63/EU/, 90/219/EEC, Regulation No. 1964/2003), as well as with the Spanish National and Regional Guidelines for Animal Experimentation (RD 53/2013 and 178/2004, Ley 32/2007 and 9/2003, Decreto 320/2010).

2.5. Evaluation of EAE clinical signs

The clinical parameters analyzed were defined as follows: (i) the day of onset, *i.e.*, the first day the mice exhibited a clinical score $\geq$ 0.5; (ii) the clinical score at onset; (iii) the maximum clinical score ("peak"); (iv) the day when animals reached their peak; (v) the severity index (SI), quantified as the ratio of the maximum clinical score and the number of days elapsed from onset to peak (Melero-Jerez et al., 2020); (vi) the recovered score (the maximum clinical score minus the final score); (vii) the percentage of recovery [(the recovered score x 100) / the maximum clinical score]; (viii) the recovery index [(the maximum clinical score minus the final score) / the number of days elapsed from peak to chronification]; and (ix) the final score, defined as the clinical score at the end of the follow-up period.

2.6. BrdU/EdU incorporation and follow-up in EAE mice

At the individualized onset of the clinical signs of each animal, BrdU (50 mg/kg in sterile 1× Phosphate Buffered Saline - PBS) was administered intraperitoneally (ip) twice a day for 3 consecutive days in the first animal cohort ($n = 12$) or until the peak of the clinical course in the second animal cohort (n = 12). In the second cohort, once the animals reached the peak, following a 24 h washout period, EdU was administered ip (50 mg/kg in PBS) twice a day during 3 consecutive days. After EdU administration, animals were sacrificed once they reached their maximal functional recovery (chronification: when they maintained the same score at least for 4 consecutive days).

2.7. Flow cytometry analysis of peripheral blood

Blood was collected from the submandibular vein of isofluorane-anesthetized mice at disease onset and at the peak of the clinical course into 2 % EDTA tubes. Erythrocytes were then lysed in a 15-mL tube with 2.5 mL ACK lysis buffer: 8.29 g/L NH4Cl; 1 g/L $KHCO_3$; 1 mM EDTA in distilled H_2O at pH 7.4 (Panreac). Subsequently, the lysis reaction was stopped by adding PBS and the blood cells were recovered by centrifugation at 210*g* for 5 min at RT. Fc cell receptors were then blocked for 10 min at 4 °C with an anti-CD16/anti-CD32 antibodies (10 μg/mL: BD Biosciences 553,142) and the cells were resuspended in 25 μL

of staining buffer: PBS supplemented with 10 % heat-inactivated fetal bovine serum (FBS: Capricorn; 25 mM), 2.5 % HEPES buffer (Gibco), 2 % Penicillin/Streptomycin (P/S: Gibco) and 0.2 % EDTA (Sigma; 0.5 M). The cells were further labeled for 30 min at 4 °C in the dark with the following fluorochrome-conjugated monoclonal antibodies, diluted in 25 μL of staining buffer: rat anti-mouse Ly-6C-FITC (10 μg/mL, AL-21 clone), rat anti-mouse Ly-6G-PE (4 μg/mL, 1A8 clone), rat anti-mouse CD11b-PerCP-Cy5.5 (4 μg/mL, M1/70 clone: all from BD Biosciences), rat anti-mouse MHC-II-PE-Cy7 (4 μg/mL, M5/114.15.2 clone), hamster anti-mouse CD11c-APC (4 μg/mL, N418 clone), and rat anti-mouse F4/80-eFluor450 (4 μg/mL, BM8 clone) to stain myeloid cells (eBioscience-Thermo Fisher Scientific). The blood cells were then rinsed with staining buffer, recovered by centrifugation at 210*g* for 5 min and fixed with 4 % PFA in PB for 10 min at RT. Analysis was performed in a FACS Canto II cytometer (BD Biosciences) at the Flow Cytometry Core Facility of the *Hospital Nacional de Parapléjicos*. The data obtained were analyzed by using the FlowJo 10.6.2 software (Tree Star Inc.).

2.8. Tissue sampling and immunohistochemistryfor murine tissue

Animals were transcardially perfused with 2 % PFA and their spinal cords were dissected out and post-fixed for 4 h at RT in the same fixative. After immersion in 30 % (*w/v*) sucrose in PB for 12 h, serial coronal cryostat sections (Leica, Nussloch) were thaw-mounted on Superfrost® Plus slides and stored at −20 °C until use (20 μm thick per section, 9 sections per slide, 7 series per animal). Spinal cord sections were air-dried for 1 h at RT. After several rinses with PB, the sections were pre-incubated for 1 h at RT in blocking buffer: 5 % normal donkey serum (NDS, Vector) and 0.2 % Triton X-100 (Merck) diluted in PBS. IHC was carried out by incubating the sections overnight at 4 °C with the following primary antibodies diluted in blocking buffer: rabbit anti-NG2 (1:200; AB5320, Millipore), mouse anti-CC1 (1:200; OP80, Calbiochem) and rabbit anti-Olig2 (1:200; AB9610, Millipore). The sections were kept for 30 min at RT and, after rinsing, antibody binding was detected with the corresponding fluorescent secondary antibodies in incubation buffer for 1 h at RT (1:1000, Invitrogen). The sections were fixed with 4 % PFA for 10 min at RT. After several rinses with 0.1 % Triton X-100 in PBS (PBST), the tissue was incubated in HCl 2 N solution (Fisher) for 30 min at 37 °C, then rinsed in borate buffer (0.1 M boric acid in distilled H_2O, pH 8.5; Sigma-Aldrich) for 10 min and then rinsed several times with PBST. The sections were incubated for 1 h at RT in incubation buffer: 5 % NDS diluted in PBST. Sections were then incubated overnight at 4 °C with sheep anti-BrdU (1:1000; ab1893, Abcam) diluted in incubation buffer. The sections were kept for 30 min at RT and, after rinsing with PBST, antibody binding was detected with the corresponding fluorescent secondary antibody in incubation buffer for 1 h at RT (1:1000, Invitrogen). The sections were rinsed again with PBST and PBS, and fixed with 4 % PFA for 10 min at RT. Then, the detection of Arginase-I (Arg—I) or EdU was performed as follows: Arg-I IHC was carried out by using a goat anti-Arg-I antibody (1:50; sc-18,351, Santa Cruz Biotechnology) and EdU was revealed using Click-iT Alexa Fluor 488 Imaging Kit according to the manufacturer's instructions (C110337, Invitrogen). The cell nuclei were stained with Hoechst 33342 (10 μg/mL, Sigma-Aldrich) and the sections were mounted with Fluoromount-G (Southern Biotech).

2.9. Image acquisition and histopathological analysis of murine tissue

Cell quantification was carried as described previously (Melero-Jerez et al., 2021). Briefly, 3 sections from one of the slides (separated by 420 μm) from each thoracic spinal cord were selected from each cohort of 12 EAE mice. A mosaic composition was created from 20× images of sections acquired on a confocal SP5 microscope (Leica) connected to a resonant scanning system at the Microscopy and Image Analysis Core Facility of the *Hospital Nacional de Parapléjicos*. Regions of interest corresponding to the demyelinated area or 'lesion', the 'perilesion' area and the adjacent non-demyelinated white matter (WM) were defined primarily by the density of the cell nuclei within the infiltrated area. Thus, the 'lesion' was determined by a high nuclear density, while the 'perilesion' was defined as the area corresponding to a 100 μm perimeter measured from the lesion edge to the adjacent area. WM was established as the area corresponding to a perimeter of 100 μm measured from the edge to the perilesion to the deep white matter. Quantification of cell density was manually performed using Image J software.

2.10. Statistical analysis

Data were expressed as mean ± SEM and analyzed using Sigma Plot version 11.0 (Systat Software Inc.), and *GraphPad Prism* statistical software (version 8.0; GraphPad software). A correlogram was generated by using *R* software version 4.2.2. Shapiro-Wilk normality tests were performed on human and murine tissue samples. A Student's *t*-test was used to compare different groups of mice (parametric statistical variables with a normal distribution) or Mann-Whitney *U* test was used for comparing non-parametric or non-normally distributed parametric variables. One-way analysis of variance (ANOVA) test or its corresponding ANOVA on ranks, followed by the appropriate *post-hoc* test, were carried out to compare between different areas of the lesions in mice or MS tissue. A Spearman's test was carried out for the correlation analyses between disease duration/age/*time postmortem* and the ratio of OPC density in MS tissue, as well as between peripheral blood M-MDSC content and the clinical signs in the EAE model. A Pearson test was used to correlate the density of OPC and the density of M-MDSCs in human samples, and the content of circulating M-MDSC and OPC/OL densities in the lesions of EAE mice. Statistical significance was set at $p < 0.05$: $^{\$}p < 0.05$, $^{\$\$}p < 0.01$, $^{\$\$\$}p < 0.001$, when comparing different animal groups ($^{\$}p < 0.05$ was also set as the difference between $NG2^+$ cell density in the rAIL of MS patients with longer *vs.* shorter disease durations); $^{*}p < 0.05$when comparing rAIL and NAWM *vs.* cAIL in human tissue, and perilesion or WM to the lesion in mice; $^{\#}p < 0.05$ when comparing lesionor WM to the perilesion in mice; $^{*}p < 0.05$, $^{**}p < 0.01$, $^{***}p < 0.001$ for correlations described in the heat map correlogram.

3. Results

3.1. Disease duration is associated to the presence of an OPC gradient in mAIL of MS patients

Previous reports have shown that the density of OPCs varies between different regions of demyelinating plaques, the surrounding periplaque and NAWM, finding either higher or lower numbers compared to the control white matter (Cui et al., 2013). To investigate whether the variables sex, clinical form of MS, or disease severity influence the relative abundance of OPCs in relation to the different inflammatory environments of MS lesions, we analyzed the cAIL, rAIL and NAWM of mAIL from 8 MS patients(Fig. 1A-F; Table 1). No significant differences were observed in OPC density between males and female patients or between SPMS/PPMS patients across any of the three regions (Table 2). In line with this, the distribution pattern of $NG2^+$ cells across different regions of mAIL was consistent regardless of sex or clinical form of MS, with the adjacent NAWM displaying a higher density of OPCs than the cAIL (Fig. 1G, H).A similar abundance of OPCs was observed in patients with longer disease durations (Fig. 1I). In contrast, in MS patients with a shorter disease duration the abundance of OPCs was lower in the rAIL compared to those with a longer disease course (Table 2, Fig. 1I). Accordingly, patients with a shorter disease course showed a higher OPC density in the adjacent NAWM compared to both the cAIL and rAIL (Fig. 1I). Correlation analyses indicated that disease duration was independent of the OPC density ratio between adjacent NAWM and the other two regions, *i.e.*, adjacent NAWM/rAIL ($r = -0.405$, $p = 0.290$) and adjacent NAWM/cAIL ($r = 0.476$, $p = 0.207$). Interestingly, we found a positive association between the ratio rAIL/cAIL of the OPC

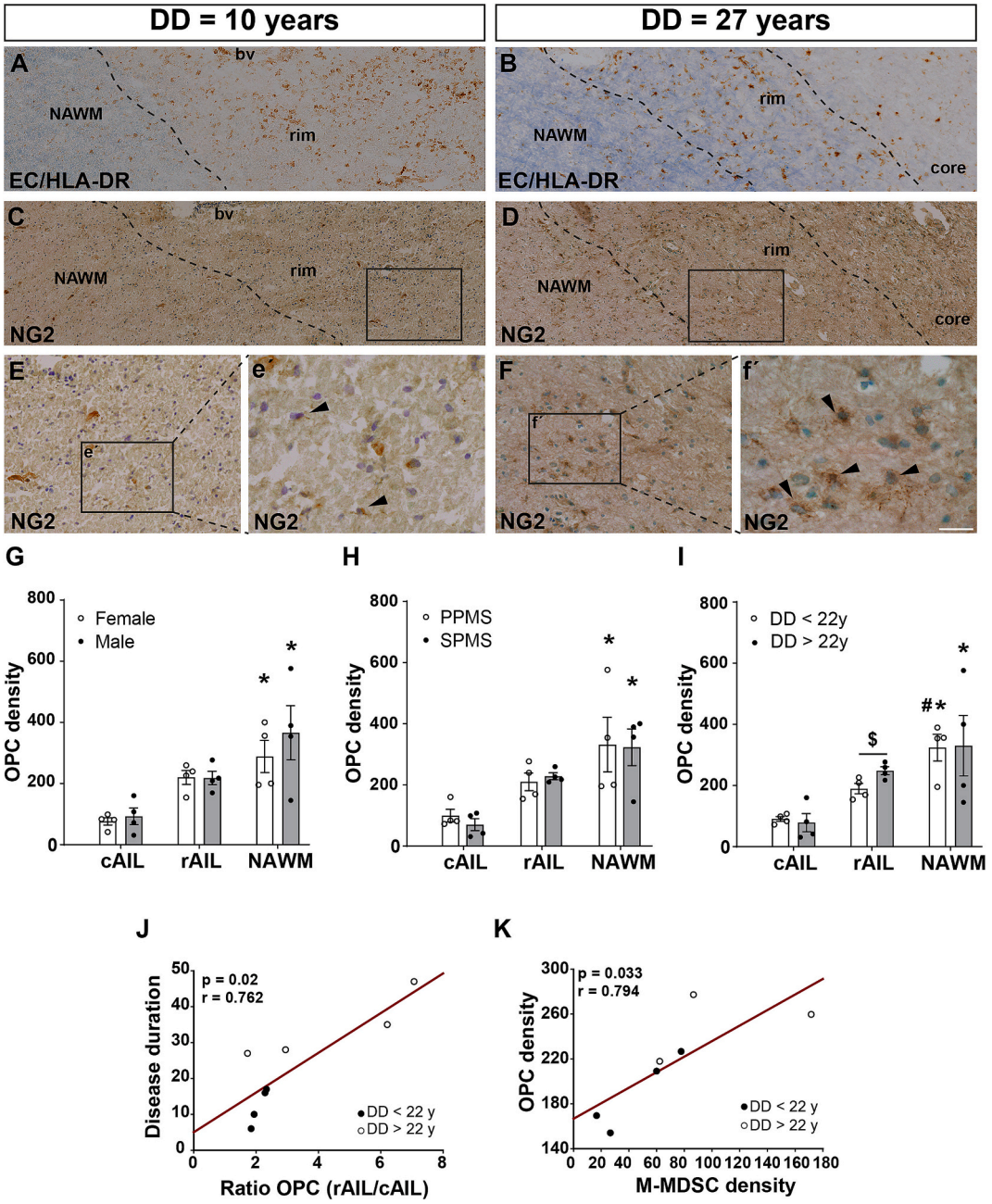

Fig. 1. Disease duration affects the abundance of OPCs associated to mAIL in MS patients. A-F: Representative images of parallel sections of two mAIL from a MS patient with short (A, C) and long (B, D) disease durations showing myelin stained with EC (blue) and inflammatory cells immunostained with anti-HLA-DR (brown) in A, B, and OPCs identified as $NG2^+$ cells in C-F: Magnification of the squared representative areas of the rim (e', f') of the same patients showing OPCs pointed with arrowheads. G-H: Quantification of MS tissue samples showing a higher density of OPCs in the adjacent NAWM compared to the cAIL, regardless of sex (G, $n = 4$ males and 4 females) or the clinical forms (H; $n = 4$ SPMS and 4 PPMS). I: OPC density was significantly lower in the rAIL of MS patients with shorter disease durations (n = 4 with long and 4 with short disease courses). J: Longer disease durations were associated with higher rAIL/cAIL ratios of OPC density ($n = 8$). G: The density of M-MDSCs in the rAIL was associated to a greater density of OPCs in the same area ($n = 7$).*$p < 0.05$, and $^{\#}p < 0.05$ when comparing the $NG2^+$cell density of an area with respect to the cAIL or the rAIL within a specific group of patients, respectively. $^{\$}p < 0.05$ when comparing $NG2^+$ cell density between patients with longer *vs.* shorter disease durations. Scale bar: A-D = 200 μm; *E*-F = 50 μm; e', f' = 20 μm.bv, blood vessel; DD, disease duration. Rest of abbreviations as in the text. Densities represent the number of $NG2^+$cells/mm^2. (For interpretation of the references to colour in this figure legend, the reader is referred to the web version of this article.)

density and disease duration (Fig. 1J) and age ($r = 0.805$, $p = 0.009$), but not with time *post-mortem* ($r = 0.500$, $p = 0.217$). The ratios of OPC density observed in adjacent NAWM/rAIL or adjacent NAWM/cAIL did not correlate either with either time *post-mortem* or age (data not shown). We previously reported a direct relationship between the density of M-MDSCs and OPCs in the demyelinated spinal cord lesions of mice with EAE (Melero-Jerez et al., 2021). Cells exhibiting all the characteristic markers of M-MDSCs, namely $CD11b^+CD33^+HLA\text{-}DR^{-/low}CD14^+CD15^-$, were recently identified in association with demyelinated plaques in MS patients (Ortega et al., 2023). Since all $CD14^+$ cells were $CD15^-$, $CD33^+$, $CD11b^+$, and $TMEM119^-$, M-MDSCs can be identified and quantified as $CD14^+CD15^-HLA\text{-}DR^{-/low}$ cells in human tissue. Within mAIL, M-MDSCs were mainly present in the rAIL of progressive MS patients (Ortega et al., 2023). Of note, the higher the density

Table 2
NG2$^+$ cell distribution in the mAILs of MS patients.

		Male	Female	*p* value	SPMS	PPMS	*p* value	DD < 22 ys	DD > 22 ys	*p* value
CELL DENSITY*	cAIL	92.97 ± 27.50	76.46 ± 12.97	0.603	99.57 ± 19.58	69.86 ± 20.49	0.335	90.76 ± 7.85	78.66 ± 29.40	0.705
	rAIL	218.40 ± 22.26	220.04 ± 23.02	0.961	228.30 ± 11.05	210.14 ± 29.14	0.886	189.79 ± 16.88	248.65 ± 12.79	0.030
	NAWM	366.38 ± 88.39	288.26 ± 52.86	0.477	322.92 ± 59.96	331.72 ± 89.53	0.938	324.02 ± 43.48	330.62 ± 98.62	0.953
RATIO#	cAIL/rAIL	3.26 ± 1.27	3.32 ± 0.98	0.886	4.37 ± 1.32	2.21 ± 0.27	0.343	2.1 ± 0.12	4.48 ± 1.27	0.343
	NAWM/ rAIL	4.19 ± 0.34	4.49 ± 1.17	0.486	5.37 ± 1.42	3.31 ± 0.59	0.230	3.61 ± 0.51	5.08 ± 1.56	0.400
	NAWM/ cAIL	1.67 ± 0.34	1.30 ± 0.17	0.343	1.41 ± 0.25	1.59 ± 0.31	0.710	1.7 ± 0.17	1.28 ± 0.32	0.300

Data are showed as the mean ± SEM. * Cell density quantified as the number of NG2$^+$ cells/mm^2. #Quantified as the ratio between the NG2$^+$ cell densities of both areas. DD: disease duration; ys: years. Rest of abbreviations as in the main text.

of M-MDSCs, the higher the abundance of OPCs in the rAIL (Fig. 1K). Overall, these results indicate that disease severity negatively affects the abundance of OPCs present in the rAIL of mAIL from MS patients. Conversely, the greater presence of the immunoregulatory M-MDSCs in the rAIL was positively associated with an enrichment of OPCs in the same area.

3.2. The severity of the effector phase of EAE influences the abundance of M-MDSCs and OPCs in the demyelinated spinal cord

In order to investigate how the distribution of M-MDSCs and OPCs in the CNS of mice with EAE affects disease severity, we took advantage of the highly translatable individualized evaluation of this animal model (Camacho-Toledano et al., 2022; Ortega et al., 2023). In a first cohort of 12 mice, the SI of EAE mice three days after disease onset ranged from 0.19 to 0.81, with a median of 0.64 (IQR 0.34–0.75). Animals were classified as mice with mild or severe EAE ($n = 6$ for each group), according to the median of the SI (Melero-Jerez et al., 2020).

We aimed to evaluate the impact of the disease severity on the distribution of M-MDSCs and the level of OPC proliferation in the demyelinated spinal cord during the effector phase of EAE. To achieve this, mice were administered BrdU for 3 consecutive days, starting at the specific disease onset of each animal, followed by the histopathological analysis of the spinal cord one day later (Fig. 2A).At the peak of EAE, Arg—I$^+$ cells within the lesion are identified in the spinal cord as M-MDSCs, all presenting the bona-fide markers of this regulatory cell type: Arg-I$^+$CD11b$^+$Gr-1$^+$CD115$^+$Ly-6B.2$^-$CD124$^+$MHC-II$^{-/low}$(Melero-Jerez et al., 2019; Moliné-Velázquez et al., 2014; Moliné-Velázquez et al., 2011). Regardless of disease severity, Arg—I$^+$ cells were more abundant in the lesion (M-MDSCs) compared to Arg—I$^+$ cells in the WM (Fig. 2B, F, J), while OPCs (NG2$^+$ cells) were predominantly found in the surrounding perilesion (Fig. 2C, G, K). Moreover, proliferating OPCs (NG2$^+$BrdU$^+$ cells) were also more present in the perilesion area compared to the lesion irrespective of the disease severity. However, OPCs that incorporated BrdU during the effector phase were significantly more abundant in the perilesion than in the adjacent WM, but only in the case of mice with mild EAE (Fig. 2D, E, H, I, L). Importantly, the severity of the effector phase drastically affected all of the cell populations mentioned above. M-MDSCs in the lesion, as well as total and proliferating OPCs in the perilesion, were more abundant in mice with a milder clinical course of EAE compared to those with severe EAE (Fig. 2J-L). Consequently, we found that the milder clinical course according to the SI, the higher density of M-MDSCs in the lesion, and of total and proliferating OPCs in the perilesion (Fig. 3; Sup. Fig. 1A-C). Therefore, these results indicate that the severity of the effector phase of the EAE clinical course negatively impacts the abundance and proliferative state of OPCs within the demyelinated CNS. Similarly, a milder disease severity positively impacts the higher abundance of immunoregulatory M-MDSCs within the inflamed spinal cord lesions.

3.3. M-MDSC abundance is directly related to higher OPC generation in the spinal cord of EAE mice

To explore the relationship between infiltrated M-MDSCs and OPC proliferative activity, we correlated the density of M-MDSCs in the lesion, *i.e.*, the area where Arg—I$^+$ cells were described as M-MDSCs, and the density of proliferating OPCs in the different areas of the infiltrated regions. We observed a direct correlation between the density of M-MDSCs and the density of proliferating OPCs both in the lesion and in the perilesion (Fig. 3; Sup. Fig. 1D-E) but not in the WM ($r = 0.308$, $p = 0.317$). Importantly, we also observed a direct correlation between M-MDSC abundance in the lesion area and a gradient of proliferating OPCs between the perilesion and the adjacent WM (Fig. 3; Sup. Fig. 1F). Therefore, the presence of M-MDSCs in the lesion is directly related to higher proliferative activity of OPCs in the closely related areas at the end of the effector phase of EAE.

We wanted to evaluate the ability of circulating M-MDSCs as biomarkers of OPC density and proliferative activity within the inflamed spinal cord of EAE mice. First, we confirmed that the higher abundance of M-MDSCs in peripheral blood at the onset of EAE, the milder disease courses according to the SI ($r = -0.775$, $p < 0.01$; Ortega et al., 2023). Interestingly, we found that the greater abundance of M-MDSCs in peripheral blood at disease onset, the more density of these cells in the lesion areas at the peak of the disease ($r = 0.762$, $p < 0.01$). With respect to OPCs, the circulating M-MDSC load at disease onset tended to correlate with the higher abundance of total and proliferating OPCs both in the lesion ($r = 0.497$, $p = 0.09$, for total OPCs; and $r = 0.538$, $p = 0.07$, for proliferating OPCs) and in the perilesion ($r = 0.531$, $p = 0.07$, for total OPCs), nearly reaching significance in the case of proliferating OPCs ($r = 0.566$, $p = 0.05$). In sum, central and peripheral M-MDSCs are positively associated with a higher content of total and newly generated OPCs in spinal cord lesions at the end of the pro-inflammatory phase of EAE.

3.4. The density of OPCs in demyelinated EAE lesions at the end of the recovery phase is independent of disease severity

In the next step, we wondered whether the impact of EAE severity on the distribution of OPCs generated during the effector phase or at the beginning of the recovery phase of EAE might still be observable in demyelinating spinal cord areas once each animal reached its maximal clinical recovery (Fig. 4A). To this aim, a second cohort of mice with EAE ($n = 12$) was again distributed in two different groups according to the median of the SI [ranging from 0.50 to 0.83, with a median of 0.69 (IQR = 0.60–0.75)]. Following the same criteria as for the first animal cohort, animals with a SI < median were classified as mice with mild EAE ($n = 5$), while those with a SI > median were classified as mice with severe EAE ($n = 7$).In this new cohort, we traced cell division during both the entire effector and the beginning of the recovery phases of EAE by injecting BrdU from the onset until the peak of the disease, and then EdU

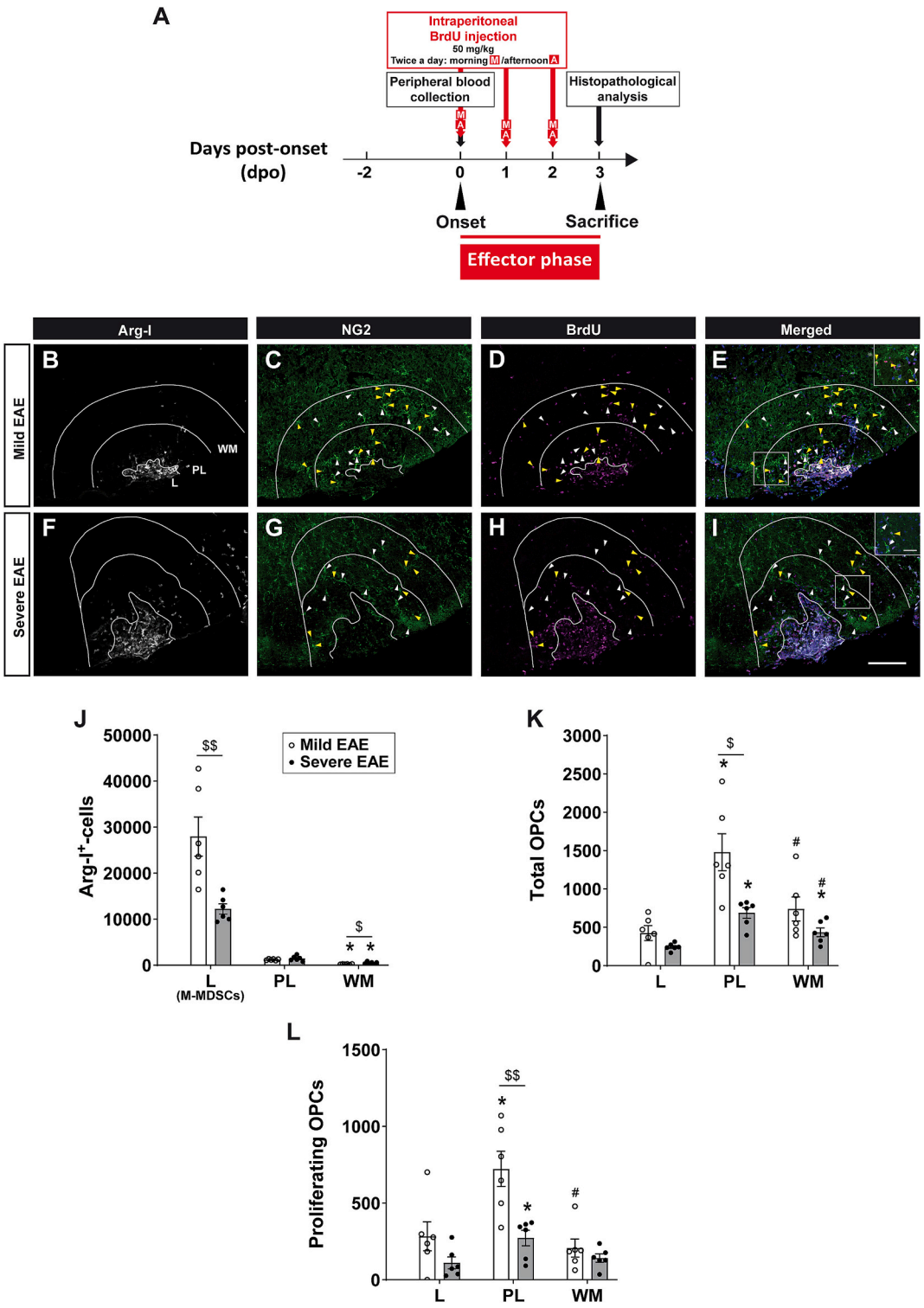

Fig. 2. Disease severity impacts on M-MDSC presence and OPC generation and distribution within the demyelinated CNS at the peak of EAE. A: Diagram representing the experimental procedure. B-I: Representative confocal images showing the distribution of M-MDSCs (Arg—I^+ cells, white), total OPCs ($NG2^+$ cells, green, pointed with white arrows) and proliferating OPCs ($BrdU^+NG2^+$ cells, magenta, pointed with yellow arrows) in the lesion (L), perilesion (PP) and adjacent white matter (WM) within the spinal cord of a mouse with a mild (B-E) or a severe (F—I) EAE. White lines indicate L, PL, and WM borders. The ventral part is at the bottom and the lateral part is on the right. J-L: The density of M-MDSCs at the L (J), total OPCs (K), and proliferating OPCs (L) at the PL was higher in mice with a mild EAE compared to those with a severe disease course. $^{\$}p < 0.05$; $^{\$\$}p < 0.01$, when comparing cell density between mice with mild *vs.* severe EAE; $^{*}p < 0.05$, and $^{\#}p < 0.05$ when comparing the cell density of an area with respect to the L or when comparing cell density of WM *vs.* the PL within a specific group of mice, respectively. Insets in E, I are higher magnifications of the white squares. Scale bar in B-*I* = 100 μm (20 μm in the insets). Densities represent the number of cells/mm^2. (For interpretation of the references to colour in this figure legend, the reader is referred to the web version of this article.)

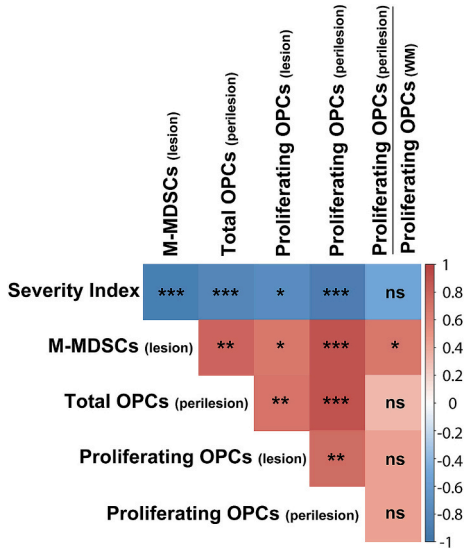

Fig. 3. Correlogram showing the association between M-MDSC, OPC abundance and disease severity in the spinal cord of EAE mice at the peak of the clinical course. The higher severity of the effector phase of EAE was inversely correlated with the density of M-MDSCs in the lesion, and the density of total OPCs and proliferating OPCs in the perilesion. The higher density of M-MDSCs in the lesion, the higher density of proliferating OPCs in the lesion and in the perilesion. M-MDSC distribution was also associated with a gradient of proliferating OPCs between the perilesion and the adjacent WM. Spearman correlation test was carried out ($n = 12$).

in the same manner for 3 consecutive days (Fig. 4B). Once the animals reached their maximal functional recovery, we quantified the density of total OPCs ($NG2^+$ cells) and the density and percentage of proliferating OPCs that came from both the effector phase ($NG2^+BrdU^+$cells) or from the early recovery phase ($NG2^+EdU^+$ cells; Fig. 4C-I). Unlike that observed at the peak of EAE, we did not observe any difference in OPC distribution between regions in the inflammatory areas of both groups of animals with mild and severe disease courses, except for a higher abundance of total OPCs in the WM compared to the lesion in mice with severe EAE (Fig. 4M). Moreover, the densities of total OPCs and proliferating OPCs were not different between mild and severe EAE mice (Fig. 4M, N). Consequently, the percentage of proliferating OPCs and the ratio between proliferating and non-proliferating OPCs were also similar in animals with high or low severity of their clinical course (Fig. 4O, P). These findings suggest that OPC abundance in the demyelinated inflammatory spinal cord regions, following maximal clinical recovery, does not reflect prior EAE severity.

3.5. Mature oligodendrocyte generation in the spinal cord influences disease severity of EAE mice

We wanted to assess the influence of OL generation on the demyelinated spinal cord in the disease severity of EAE mice. Once the animals had reached their maximal functional recovery, we quantified the density of total OLs ($CC1^+Olig2^+$ cells), newly generated OLs during the whole effector phase ($CC1^+Olig2^+BrdU^+$) or during the early recovery phase ($CC1^+Olig2^+EdU^+$ cells), and surviving OLs ($CC1^+Olig2^+BrdU^-EdU^-$ cells; Fig. 5A-J). We did not find any difference in the cellular densities of total or surviving OLs within the perilesion of animals with mild or severe EAE (total OLs: mild EAE = 430.11 ± 83.02, severe EAE = 278.34 ± 40.49, $p = 0.102$; surviving OLs: mild EAE = 299.13 ± 59.41, severe EAE = 219.00 ± 29.39, $p = 0.215$). Interestingly, we found an increased production of OLs in the perilesion of mice with milder disease courses, irrespective of the clinical phase of origin (Fig. 5K, L). In general, the percentage of newly generated OLs with respect to the total OL population was higher in the perilesion of mice with mild EAE than in those with severe EAE (Fig. 5M). Of note, the ratio between newly generated OLs and surviving OLs was also higher in the perilesion of EAE animals with milder disease courses (Fig. 5N). Additionally, the higher the ratio of newly generated OLs in the perilesion or lesion areas relative to the WM, the greater the functional recovery exhibited by EAE animals (Fig. 5O, P). Overall, these results indicate that OL generation in the perilesion of spinal cord demyelinated areas importantly affects disease severity of EAE mice.

3.6. Circulating M-MDSC load is indicative of the future production of mature OLs in spinal cord demyelinated lesions

We previously reported that peripheral blood M-MDSCs at the onset of the EAE are associated with milder disease courses and less demyelination and axonal damage in the spinal cord of EAE mice (Ortega et al., 2023). Here, we corroborated the inverse correlation between circulating M-MDSC load in the blood at disease onset and the future SI ($r = -0.582$, $p < 0.05$). Moreover, we found for the first time that the higher the abundance of M-MDSCs in peripheral blood at onset, the higher the recovery index ($r = 0.633$; $p < 0.05$), which is indicative of a faster reduction of EAE symptoms. Finally, we confirmed that the higher the load of circulating M-MDSCs at the peak of the disease, the greater and faster the recovery of EAE mice (percentage of recovered score: $r = 0.664$, $p < 0.05$; recovery index: $r = 0.692$, $p < 0.05$). These results show that the abundance of circulating M-MDSCs both at the onset and at the peak of the disease is indicative of a better symptom recovery.

We next explored the predictive ability of circulating M-MDSCs for the presence and generation of OPCs and OLs in the lesion and the perilesion areas at the end of the recovery phase. Regarding OPCs, we did not find any correlation between the percentage of circulating M-MDSCs at onset or peak of EAE with the density of total or proliferating OPCs both in the lesion and in the perilesion of the inflammatory areas (data not shown). On the contrary, the proportion of circulating M-MDSCs at EAE onset directly correlated with a lesion enriched in newly generated OLs at the end of the recovery phase (Fig. 6A). Interestingly, the abundance of circulating M-MDSCs at the peak of EAE was directly associated with the percentage of newly generated OLs (Fig. 6B), as well as with the enrichment of newly generated OLs in the perilesion (Fig. 6C). These data indicate that the proportion of M-MDSCs in peripheral blood of mice with EAE can give information about the future greater ability of the CNS to produce mature OLs associated with demyelinated areas.

4. Discussion

Inefficient remyelination in MS leads to neurodegeneration, which is closely related to the permanent disability observed in MS patients (Boyd et al., 2013; Kornek et al., 2000). To date, the available treatments for MS are indicated for reducing disease activity (relapses) or the associated symptoms but do not tackle neurodegeneration. Hence, there is an urgent need for the search of novel compounds that enhance myelin regeneration and prevent the associated axonal degeneration (Lubetzki et al., 2020). Despite the large variety of pro-remyelinating candidate drugs, only a few have reached Phase 2 clinical trials. However, those trials conducted in RRMS patients have shown limited or no clinical improvements (Cadavid et al., 2019; Diebold and Derfuss, 2019; Schwartzbach et al., 2017). The influence of the heterogeneity described in human oligodendroglial cells across MS patients (Jäkel et al., 2019) on their ability to generate new myelin following demyelination has yet to be fully elucidated. Recent studies point newly generated OLs as more efficient at remyelination than those that survive demyelination (Mezydlo et al., 2023; Neely et al., 2022). Therefore, identifying suitable biomarkers that enable more precise classification of MS patients based on their ability to generate new myelinating oligodendrocytes could contribute to the success of clinical trials with pro-remyelinating drugs.

In the present work, we observe that OPC density in the rAIL is higher

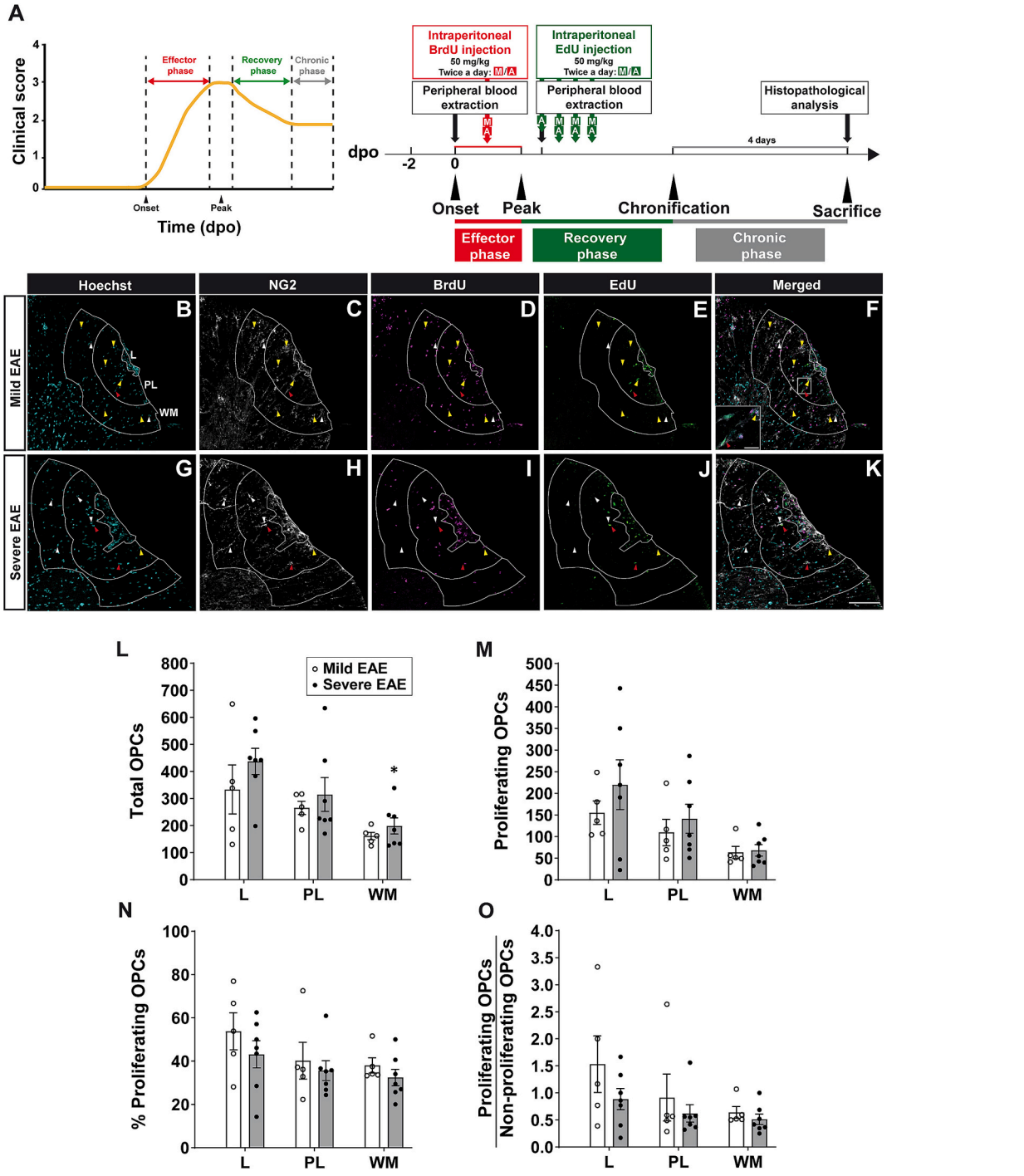

Fig. 4. Disease severity does not mirror the distribution of OPCs present in the demyelinated spinal cord at the end of the recovery phase. A: Schematic representation of the different phases of the EAE clinical course. B: Diagram representing the experimental procedure. C-L: Representative confocal images showing the distribution of total OPCs ($NG2^+$ cells, white, white arrowheads), OPCs originated during the effector phase of EAE ($NG2^+BrdU^+$ cells, magenta, yellow arrowheads) and OPCs generated during the recovery phase of EAE ($NG2^+EdU^+$ cells, green, red arrowheads), in the lesion (L), perilesion (PL) and adjacent white matter (WM) within the spinal cord of mice that experienced a mild (C-G) or severe (H-L) EAE. Cell nuclei was visualized with Hoechst (C, H). White lines indicate L, PL and WM borders. Ventral is on the right and lateral is on the top. M, N: Quantification of total (L) and proliferating OPCs (M) densities did not reveal any difference between EAE groups. Mice with severe EAE exhibited a slightly greater abundance of OPCs in the WM compared to the L (M). O, P: Neither the percentage of proliferating OPCs ($NG2^+BrdU^+$ or $NG2^+EdU^+$ cells, O), nor the ratio between proliferating and non-proliferating OPCs (P) were affected by disease severity. *$p < 0.05$, when comparing the cell density of an area with respect to the L within a specific group of mice. Inset in F is a higher magnification of the white square, showing $NG2^+BrdU^+$ cells (yellow arrowheads) and $NG2^+EdU^+$ cells (red arrowheads). Scale bar in C-L = 100 μm (15 μm in the inset). Densities represent the number of cells/mm^2. (For interpretation of the references to colour in this figure legend, the reader is referred to the web version of this article.)

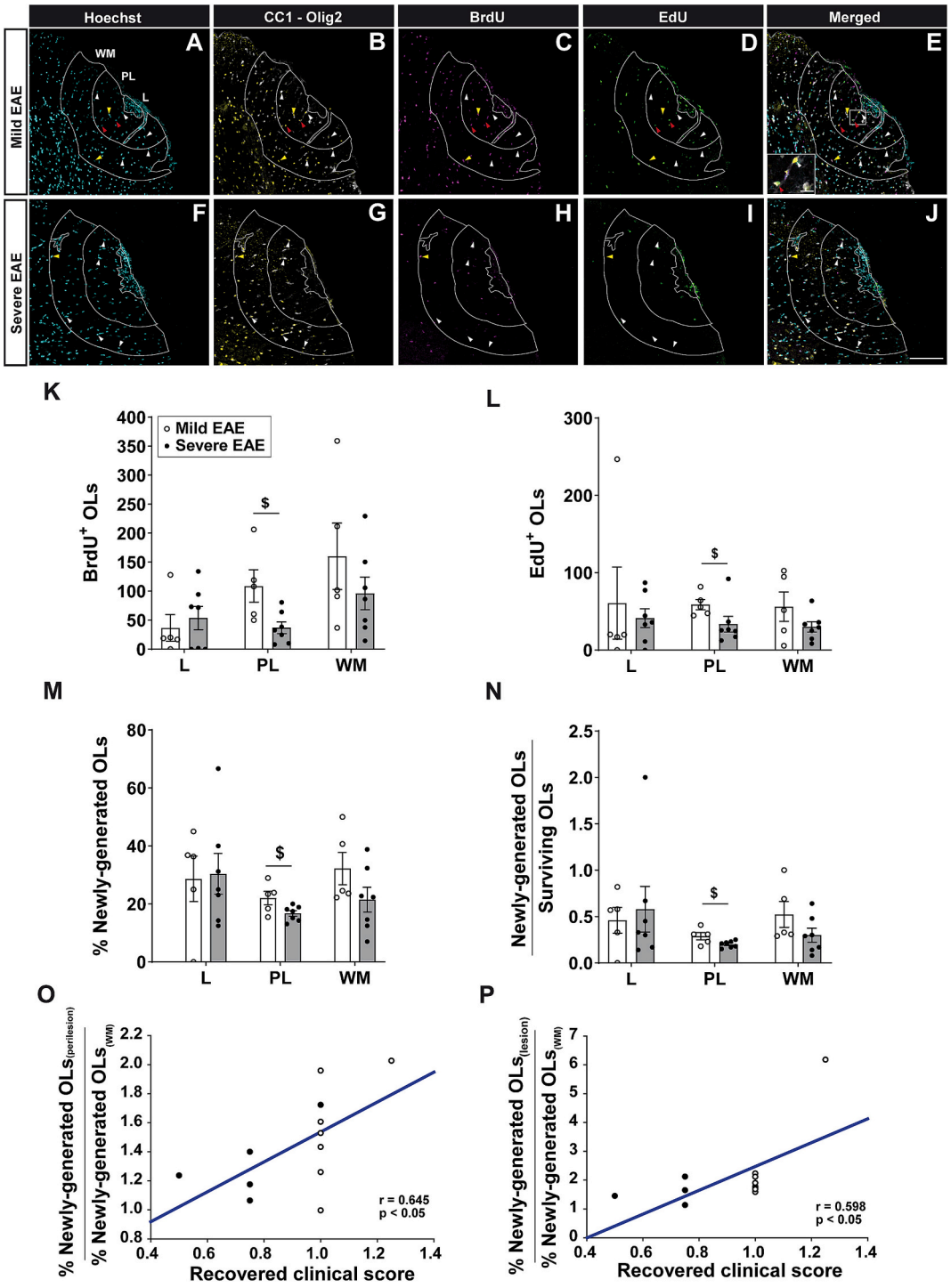

Fig. 5. The distribution of newly generated oligodendrocytes in the demyelinated spinal cord after the recovery from the inflammatory insult affects the severity of EAE. A-J: Representative confocal images showing the distribution of mature OLs ($CC1^+Olig2^+$ cells, white cytoplasm with yellow nucleus, white arrowheads), OLs originated during the effector phase of EAE ($CC1^+Olig2^+BrdU^+$ cells, white cytoplasm with magenta nucleus, yellow arrowheads) and OLs generated during the early recovery phase of EAE ($CC1^+Olig2^+EdU^+$ cells, white cytoplasm with green nucleus, red arrowheads), in the lesion (L), perilesion (PL) and adjacent white matter (WM) within the spinal cord of mice with a mild (A-E) and severe (F-J) EAE. Cell nuclei was visualized with Hoechst (A, F). White lines indicate L, PLand WM borders. Ventral is on the right and lateral is on the top. K-N: The density of $BrdU^+$ (K) and EdU^+ newly originated OLs (L) was higher in the PL of mice with mild EAE compared to those with a severe disease. M: Mice with a mild EAE presented a higher percentage of newly generated OLs ($CC1^+Olig2^+BrdU^+$ or $CC1^+Olig2^+EdU^+$ cells) in the PL than mice that experienced a severe EAE. N: The ratio between the density of newly generated and surviving OLs was also higher in the PL of mice with mild *vs.* severe EAE. O, P: The ratio between the percentage of new OLs found in the PL (O) and L (P) relative to that observed in the WM is directly associated with greater clinical recovery. $^{\$}p < 0.05$. Inset in E is a higher magnification of the white square. Scale bar: A-J = 100 μm (15 μm in the inset). Densities represent the number of cells/mm^2. (For interpretation of the references to colour in this figure legend, the reader is referred to the web version of this article.)

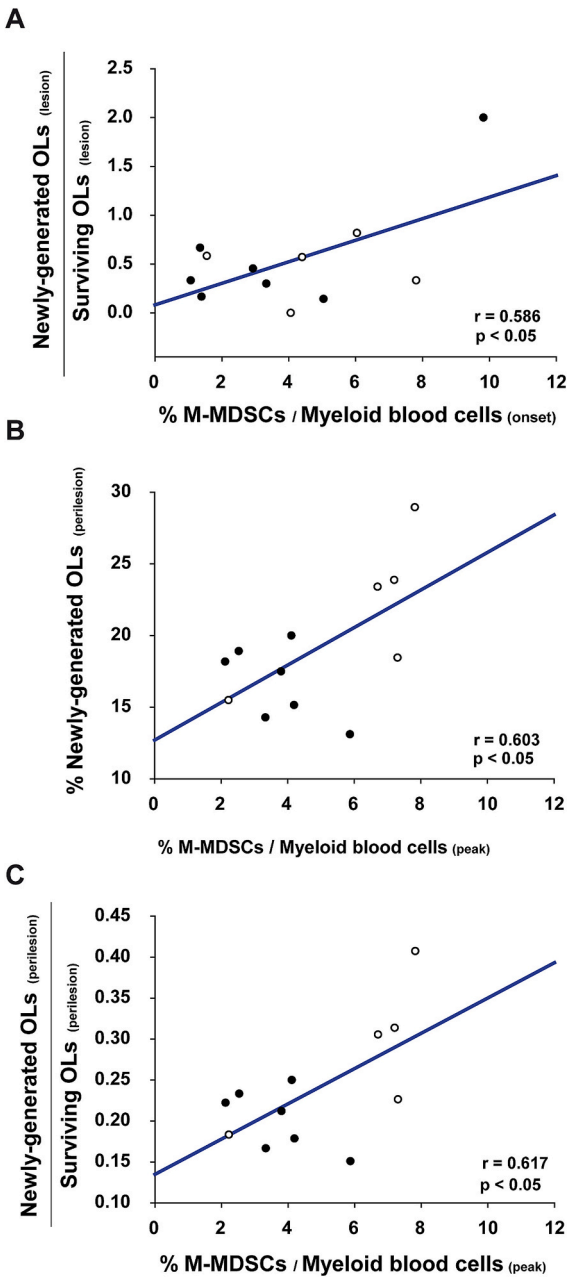

Fig. 6. Circulating M-MDSC load is indicative of a CNS prone to produce new OLs during the disease course of EAE. A: The abundance of circulating M-MDSCs at EAE onset is directly associated with a higher presence of newly generated OLs in the lesion of the infiltrated area at the end of the recovery phase. B: The higher proportion of M-MDSCs in peripheral blood at the peak of EAE, the higher percentage of newly generated OLs in the perilesion. C: The abundance of circulating M-MDSCs at the peak of EAE directly correlates with a greater enrichment of newly generated OLs in the perilesion. Pearson correlation test was carried out ($n = 12$). White circles represent mice with a mild EAE ($n = 5$); black circles represent mice with a severe EAE ($n = 7$). Densities represent the number of cells/mm^2.

in MS patients with a longer disease duration, while sex and clinical forms do not appear to be associated with differences in the distribution or abundance of OPCs. Additionally, we describe a direct correlation between disease duration and the ratio of OPC density in the rAIL to OPC density in the cAIL. These data suggest that milder forms of the disease are associated with a higher presence of OPCs in the rAIL, a finding consistent with our observations in the EAE model. In patients with progressive MS, a greater proportion of mAIL is associated with a shorter disease duration together with a shorter time to reach an expanded disability status scale (EDSS) of 6 or 8 (Luchetti et al., 2018). Therefore, our data suggest that disease severity negatively influences OPC abundance in those lesions associated to more aggressive MS courses. Moreover, we observe that the higher the density of M-MDSCs, the higher the density of OPCs in the rAIL, which is in accordance with our previous observations in the EAE model, where the presence of M-MDSCs in the demyelinated lesions directly correlated with the density of OPCs in the surrounding perilesion (Melero-Jerez et al., 2021). M-MDSCs have been recently found in highly inflammatory areas of progressive MS patients, including the rAIL. Interestingly, in PPMS patients, a lower content of M-MDSCs together with a more evidenced pro-inflammatory environment is associated with a more severe disease course (Ortega et al., 2023). Therefore, our data suggest that M-MDSCs may have a relevant role for OPC biology in the context of MS demyelinating lesions.

EAE mice exhibit a biological variability that, when evaluated individually, allows for the study of the heterogeneity of disease severity observed in MS patients (Melero-Jerez et al., 2020). Our group has shown that the individualized follow-up of the animals constitutes a good strategy for the search of biomarkers in this MS model, a scientific formula that helps to close the gap between preclinical and clinical research (Camacho-Toledano et al., 2022; Ortega et al., 2023). In the present work, the individualized monitoring of the EAE mice allow us to demonstrate that OPC distribution and self-renewal at the peak but not at the recovery phase of the disease influences EAE severity, while OPC differentiation is highly detected in animals with a mild EAE once they reached their maximal symptom recovery. Namely, at the peak of EAE, mice with a mild disease course present a greater density of total and proliferating OPCs in the perilesion of the spinal cord demyelinated areas originated during the effector phase of the disease when pro-inflammatory myeloid cells are predominant (Giles et al., 2018; Locatelli et al., 2018). This is consistent with the fact that pro-inflammatory molecules released by microglia/macrophages, but also by OPCs themselves, stimulate remyelination by enhancing OPC activation and proliferation (Arnett et al., 2001; Cunha et al., 2020; Mason et al., 2001; Moyon et al., 2015). In addition, we find a direct association between the presence of M-MDSCs at the lesion and the abundance of proliferating OPCs in the perilesion, which is in line with our previous work that describe M-MDSCs as promoters of OPC proliferation *in vitro* (Melero-Jerez et al., 2021). Furthermore, we observe a higher percentage of newly generated OLs in the perilesion from mice with a mild course of EAE originated both during the effector phase or the early immunomodulatory phase preceding symptom recovery. The latter examined period marks the switch of monocyte-derived macrophages from a pro-inflammatory to an anti-inflammatory profile (Giles et al., 2018; Locatelli et al., 2018), a cellular state with a proved ability to induce the differentiation of OPCs (Miron et al., 2013).

We previously observed that the severity of EAE is related to several histopathological hallmarks, as mice with severe disease courses present more lymphocyte infiltration, demyelination and axonal damage (Melero-Jerez et al., 2020). Thus, although a moderate inflammation is crucial to drive myelin-associated regenerative processes (Cantoni et al., 2015; Cunha et al., 2020), a persistent pro-inflammatory environment (Brambilla et al., 2014; Mei et al., 2016) together with a poor presence of cells with anti-inflammatory properties (McIntyre et al., 2020; Miron et al., 2013; Zabala et al., 2018) could contribute to OPC differentiation arrest, this being the case in the active lesions and in the rim of mAIL from MS patients (Heß et al., 2020).Remyelination is almost absent at the peak of EAE while it is observed at the chronic stage, which indicates that the regeneration of myelin fails in the presence of an exacerbated inflammation (Mei et al., 2016), something that may be reversed by pharmacologically modulated pro-inflammatory cells (Ji et al., 2024). However, an anti-inflammatory milieu able to reduce EAE severity and potentiate the immunosuppressive activity of regulatory cells as M-MDSCs, could prompt myelin regeneration, as these cells are associated

with increased T cell apoptosis (Melero-Jerez et al., 2020) and modulate OPC proliferation and differentiation (Melero-Jerez et al., 2021). In addition to the influence of the inflammatory/anti-inflammatory environment, it has been described a clear OPC heterogeneity dependent on origin, age and local environment both in homeostatic or pathological conditions (Bribián et al., 2020; Marisca et al., 2020; Sherafat et al., 2021). Therefore, we cannot rule out that pre-existing interindividual variability in OPC and/or OL density, rather than the extent of the immune response, may be the main factor influencing the endogenous capacity of each mouse to generate new oligodendroglial cells following demyelinating injury.

Notably, we find a positive relationship between circulating M-MDSCs at the onset and peak of EAE and the enrichment of newly generated OLs in the lesion and perilesion of the infiltrated areas, respectively, once each animal has reached the maximal recovery. Circulating M-MDSCs at disease onset have been shown to be an excellent biomarker of milder disease courses and less demyelination and axonal damage in the spinal cord at the end of the effector phase of EAE (Ortega et al., 2023). Moreover, it was shown that the greater the abundance of circulating M-MDSCs at the peak of EAE, the better the symptom recovery in the same MS model (Ortega et al., 2023). Thus, circulating M-MDSCs in EAE point to be not only a promising biomarker for predicting milder disease courses, but also for indicating a CNS prone to produce new OLs, whose interrelationship is highlighted in the present work.

5. Conclusions

Here, we present evidence that disease severity is associated with the abundance of OPCs in mAIL from MS patients and with the generation of OLs in the EAE animal model. Furthermore, our work shows a relationship between circulating M-MDSCs and the future OL generation in demyelinated spinal cord lesions found at the end of the clinical symptom recovery. This study provides a basis for the preclinical exploration of new biomarkers that could help identify a CNS more prone to generating new OPCs and OLs, with implications for the development of pro-myelinating treatments.

Supplementary data to this article can be found online at https://doi.org/10.1016/j.nbd.2025.106919.

CRediT authorship contribution statement

Mari Paz Serrano-Regal: Writing – original draft, Visualization, Investigation, Formal analysis. **Celia Camacho-Toledano:** Writing – original draft, Visualization, Investigation, Formal analysis. **Inmaculada Alonso-García:** Investigation, Formal analysis. **María Cristina Ortega:** Writing – original draft, Visualization, Investigation, Formal analysis. **Isabel Machín-Díaz:** Investigation. **Rafael Lebrón-Galán:** Investigation. **Jénnifer García-Arocha:** Investigation. **Leticia Calahorra:** Investigation. **Manuel Nieto-Díaz:** Formal analysis, Visualization. **Diego Clemente:** Writing – review & editing, Writing – original draft, Visualization, Supervision, Resources, Project administration, Funding acquisition, Conceptualization.

Ethics approval

This study was performed in line with the principles of the Declaration of Helsinki. Approval for human tissue study was granted by the Ethics Committee of the *Complejo Hospitalario Universitario de Toledo* (11/12/2020; No 637).

Funding

This work was supported by the *Instituto de Salud Carlos III* (PI18/00357; PI21/00302, PI24/00447, and RD16/0015/0019, co-funded by the European Union; and CB22/05/00016), *Fundación Merck Salud, Esclerosis Múltiple España* (REEM-EME_ 2018). MPS-R held a post-doctoral contract from the *Fundación del Hospital Nacional de Parapléjicos* and the *Consejería de Sanidad de Castilla-La Mancha* (EXP_04). CC-T held a predoctoral fellowship from the *Instituto de Salud Carlos III* (FI19/00132, co-funded by the European Union). MPS-R and IA-G were hired thanks to the collaborative agreement with the company EMD Serono. LC and JG-A were hired under PI18/00357 and RD16/0015/0019, respectively.

Declaration of competing interest

Diego Clemente reports financial support was provided by EMD Serono Inc. If there are other authors, they declare that they have no known competing financial interests or personal relationships that could have appeared to influence the work reported in this paper.

Acknowledgements

The authors would like to thank Dr. Virginia Vila-del Sol and Ángela Marquina Rodríguez at the Flow Cytometry Core Facility of the *Hospital Nacional de Parapléjicos* and Dr. José Ángel Rodríguez-Alfaro and Dr. Javier Mazarío at the Microscopy Core Facility of the *Hospital Nacional de Parapléjicos* for their assistance with the flow cytometry analysis and the confocal imaging and histological quantifications.

Availability of data and material

The datasets generated and/or analyzed during the current study are available in the Zenodo repository (https://zenodo.org/records/12748820).

References

Arnett, H.A., Mason, J., Marino, M., Suzuki, K., Matsushima, G.K., Ting, J.P.-Y., 2001. TNFα promotes proliferation of oligodendrocyte progenitors and remyelination. Nat. Neurosci. 4, 1116–1122. https://doi.org/10.1038/nn738.

Bodini, B., Veronese, M., García-Lorenzo, D., Battaglini, M., Poirion, E., Chardain, A., Freeman, L., Louapre, C., Tchikviladze, M., Papeix, C., Dollé, F., Zalc, B., Lubetzki, C., Bottlaender, M., Turkheimer, F., Stankoff, B., 2016. Dynamic imaging of individual remyelination profiles in multiple sclerosis. Ann. Neurol. 79, 726–738. https://doi.org/10.1002/ana.24620.

Boyd, A., Zhang, H., Williams, A., 2013. Insufficient OPC migration into demyelinated lesions is a cause of poor remyelination in MS and mouse models. Acta Neuropathol. 125, 841–859. https://doi.org/10.1007/s00401-013-1112-y.

Brambilla, R., Morton, P.D., Ashbaugh, J.J., Karmally, S., Lambertsen, K.L., Bethea, J.R., 2014. Astrocytes play a key role in EAE pathophysiology by orchestrating in the CNS the inflammatory response of resident and peripheral immune cells and by suppressing remyelination. Glia 62, 452–467. https://doi.org/10.1002/glia.22616.

Bribián, A., Medina-Rodríguez, E.M., Josa-Prado, F., García-Álvarez, I., Machín-Díaz, I., Esteban, P.F., Murcia-Belmonte, V., Vega-Zelaya, L., Pastor, J., Garrido, L., de Castro, F., 2020. Functional heterogeneity of mouse and human brain OPCs: relevance for preclinical studies in multiple sclerosis. J. Clin. Med. 9, 1681. https://doi.org/10.3390/jcm9061681.

Bronte, V., Brandau, S., Chen, S.-H., Colombo, M.P., Frey, A.B., Greten, T.F., Mandruzzato, S., Murray, P.J., Ochoa, A., Ostrand-Rosenberg, S., Rodriguez, P.C., Sica, A., Umansky, V., Vonderheide, R.H., Gabrilovich, D.I., 2016. Recommendations for myeloid-derived suppressor cell nomenclature and characterization standards. Nat. Commun. 7, 12150. https://doi.org/10.1038/ncomms12150.

Cadavid, D., Mellion, M., Hupperts, R., Edwards, K.R., Calabresi, P.A., Drulović, J., Giovannoni, G., Hartung, H.-P., Arnold, D.L., Fisher, E., Rudick, R., Mi, S., Chai, Y., Li, J., Zhang, Y., Cheng, W., Xu, L., Zhu, B., Green, S.M., Chang, I., Deykin, A., Sheikh, S.I., Agüera Morales, E., Al Khedr, A., Ampapa, R., Arroyo, R., Belkin, M., Bonek, R., Boyko, A., Capra, R., Centonze, D., Clavelou, P., Debouverie, M., Drulovic, J., Edwards, K., Evangelou, N., Evdoshenko, E., Fernández, O., Fernández Sánchez, V., Freedman, M., Freedman, S., Fryze, W., Garcia-Merino, A., Gavric-Kezic, M., Ghezzi, A., Gout, O., Grimaldi, L., Hendin, B., Hertmanowska, H., Hintzen, R., Hradilek, P., Hupperts, R., Ilkowski, J., Ivashinenkova, E., Izquierdo, G., Jacques, F., Jakab, G., Khabirov, F., Klodowska-Duda, G., Komoly, S., Kostic, S., Kovarova, I., Kremenchuzky, M., Laganke, C., LaPierre, Y., Maciejowski, M., Maison, F.G., Marfia, G.A., Martínez Yélamos, S., Meluzinova, E., Montalban, X., Murray, R., Naismith, R., Newsome, S., Nguyen, V., Oreja, D., Pardo, G., Pasechnik, E., Patti, F., Potemkowski, A., Prokopenko, S., Qian, P., Rodríguez-Antigüedad, A., Rossman, H., Rozsa, C., Sánchez López, F., Selmaj, K., Silber, E., Stepien, A., Stepniewska, A., Swiat, M., Toncev, G., Tourbah, A., Trushnikova, T., Uccelli, A., Vachova, M., Valis, M., Vecsei, L., Wiertlewski, S., Zaffaroni, M., Zielinski, T., 2019. Safety and efficacy of opicinumab in patients with relapsing

multiple sclerosis (SYNERGY): a randomised, placebo-controlled, phase 2 trial. Lancet Neurol. 18, 845–856. https://doi.org/10.1016/S1474-4422(19)30137-1.
Camacho-Toledano, C., Machín-Díaz, I., Calahorra, L., Cabañas-Cotillas, M., Otaegui, D., Castillo-Triviño, T., Villar, L.M., Costa-Frossard, L., Comabella, M., Midaglia, L., García-Domínguez, J.M., García-Arocha, J., Ortega, M.C., Clemente, D., 2022. Peripheral myeloid-derived suppressor cells are good biomarkers of the efficacy of fingolimod in multiple sclerosis. J. Neuroinflammation 19, 277. https://doi.org/10.1186/s12974-022-02635-3.
Cantoni, C., Bollman, B., Licastro, D., Xie, M., Mikesell, R., Schmidt, R., Yuede, C.M., Galimberti, D., Olivecrona, G., Klein, R.S., Cross, A.H., Otero, K., Piccio, L., 2015. TREM2 regulates microglial cell activation in response to demyelination in vivo. Acta Neuropathol. 129, 429–447. https://doi.org/10.1007/s00401-015-1388-1.
Clemente, D., Ortega, M.C., Arenzana, F.J., de Castro, F., 2011. FGF-2 and Anosmin-1 are selectively expressed in different types of multiple sclerosis lesions. J. Neurosci. 31, 14899–14909. https://doi.org/10.1523/JNEUROSCI.1158-11.2011.
Cordano, C., Sin, J.H., Timmons, G., Yiu, H.H., Stebbins, K., Guglielmetti, C., Cruz-Herranz, A., Xin, W., Lorrain, D., Chan, J.R., Green, A.J., 2022. Validating visual evoked potentials as a preclinical, quantitative biomarker for remyelination efficacy. Brain 145, 3943–3952. https://doi.org/10.1093/brain/awac207.
Correale, J., Rush, C.A., Barboza, A., 2023. Are highly active and aggressive multiple sclerosis the same entity? Front. Neurol. 14. https://doi.org/10.3389/fneur.2023.1132170.
Cui, Q.-L., Kuhlmann, T., Miron, V.E., Leong, S.Y., Fang, J., Gris, P., Kennedy, T.E., Almazan, G., Antel, J., 2013. Oligodendrocyte progenitor cell susceptibility to injury in multiple sclerosis. Am. J. Pathol. 183, 516–525. https://doi.org/10.1016/j.ajpath.2013.04.016.
Cunha, M.I., Su, M., Cantuti-Castelvetri, L., Müller, S.A., Schifferer, M., Djannatian, M., Alexopoulos, I., van der Meer, F., Winkler, A., van Ham, T.J., Schmid, B., Lichtenthaler, S.F., Stadelmann, C., Simons, M., 2020. Pro-inflammatory activation following demyelination is required for myelin clearance and oligodendrogenesis. J. Exp. Med. 217. https://doi.org/10.1084/jem.20191390.
Dendrou, C.A., Fugger, L., Friese, M.A., 2015. Immunopathology of multiple sclerosis. Nat. Rev. Immunol. 15, 545–558. https://doi.org/10.1038/nri3871.
Deshmukh, V.A., Tardif, V., Lyssiotis, C.A., Green, C.C., Kerman, B., Kim, H.J., Padmanabhan, K., Swoboda, J.G., Ahmad, I., Kondo, T., Gage, F.H., Theofilopoulos, A.N., Lawson, B.R., Schultz, P.G., Lairson, L.L., 2013. A regenerative approach to the treatment of multiple sclerosis. Nature 502, 327–332. https://doi.org/10.1038/nature12647.
Diebold, M., Derfuss, T., 2019. The monoclonal antibody GNbAC1: targeting human endogenous retroviruses in multiple sclerosis. Ther. Adv. Neurol. Disord. 12. https://doi.org/10.1177/1756286419833574, 175628641983357.
Filippi, M., Bar-Or, A., Piehl, F., Preziosa, P., Solari, A., Vukusic, S., Rocca, M.A., 2018. Multiple sclerosis. Nat. Rev. Dis. Prim. 4, 43. https://doi.org/10.1038/s41572-018-0041-4.
Franklin, R.J.M., Ffrench-Constant, C., 2017. Regenerating CNS myelin — from mechanisms to experimental medicines. Nat. Rev. Neurosci. 18, 753–769. https://doi.org/10.1038/nrn.2017.136.
Giles, D.A., Washnock-Schmid, J.M., Duncker, P.C., Dahlawi, S., Ponath, G., Pitt, D., Segal, B.M., 2018. Myeloid cell plasticity in the evolution of central nervous system autoimmunity. Ann. Neurol. 83, 131–141. https://doi.org/10.1002/ana.25128.
Heß, K., Starost, L., Kieran, N.W., Thomas, C., Vincenten, M.C.J., Antel, J., Martino, G., Huitinga, I., Healy, L., Kuhlmann, T., 2020. Lesion stage-dependent causes for impaired remyelination in MS. Acta Neuropathol. 140, 359–375. https://doi.org/10.1007/s00401-020-02189-9.
Ineichen, B.V., Kapitza, S., Bleul, C., Good, N., Plattner, P.S., Seyedsadr, M.S., Kaiser, J., Schneider, M.P., Zörner, B., Martin, R., Linnebank, M., Schwab, M.E., 2017. Nogo-a antibodies enhance axonal repair and remyelination in neuro-inflammatory and demyelinating pathology. Acta Neuropathol. 134, 423–440. https://doi.org/10.1007/s00401-017-1745-3.
Jäkel, S., Agirre, E., Mendanha Falcão, A., van Bruggen, D., Lee, K.W., Knuesel, I., Malhotra, D., Ffrench-Constant, C., Williams, A., Castelo-Branco, G., 2019. Altered human oligodendrocyte heterogeneity in multiple sclerosis. Nature 566, 543–547. https://doi.org/10.1038/s41586-019-0903-2.
Ji, X.-Y., Guo, Y.-X., Wang, L.-B., Wu, W.-C., Wang, J.-Q., He, J., Gao, R., Rasouli, J., Gao, M.-Y., Wang, Z.-H., Xiao, D., Zhang, W.-F., Ciric, B., Zhang, Y., Li, X., 2024. Microglia-derived exosomes modulate myelin regeneration via miR-615-5p/MYRF axis. J. Neuroinflammation 21, 29. https://doi.org/10.1186/s12974-024-03019-5.
Kessler, W., Thomas, C., Kuhlmann, T., 2023. Microglia activation in periplaque white matter in multiple sclerosis depends on age and lesion type, but does not correlate with oligodendroglial loss. Acta Neuropathol. 146, 817–828. https://doi.org/10.1007/s00401-023-02645-2.
Koch-Henriksen, N., Sørensen, P.S., 2010. The changing demographic pattern of multiple sclerosis epidemiology. Lancet Neurol. 9, 520–532. https://doi.org/10.1016/S1474-4422(10)70064-8.
Kornek, B., Storch, M.K., Weissert, R., Wallstroem, E., Stefferl, A., Olsson, T., Linington, C., Schmidbauer, M., Lassmann, H., 2000. Multiple sclerosis and chronic autoimmune encephalomyelitis. Am. J. Pathol. 157, 267–276. https://doi.org/10.1016/S0002-9440(10)64537-3.
Kotelnikova, E., Kiani, N.A., Abad, E., Martinez-Lapiscina, E.H., Andorra, M., Zubizarreta, I., Pulido-Valdeolivas, I., Pertsovskaya, I., Alexopoulos, L.G., Olsson, T., Martin, R., Paul, F., Tegnér, J., Garcia-Ojalvo, J., Villoslada, P., 2017. Dynamics and heterogeneity of brain damage in multiple sclerosis. PLoS Comput. Biol. 13, e1005757. https://doi.org/10.1371/journal.pcbi.1005757.
Kotter, M.R., Li, W.-W., Zhao, C., Franklin, R.J.M., 2006. Myelin impairs CNS Remyelination by inhibiting oligodendrocyte precursor cell differentiation. J. Neurosci. 26, 328–332. https://doi.org/10.1523/JNEUROSCI.2615-05.2006.
Kuhlmann, T., Miron, V., Cuo, Q., Wegner, C., Antel, J., Bruck, W., 2008. Differentiation block of oligodendroglial progenitor cells as a cause for remyelination failure in chronic multiple sclerosis. Brain 131, 1749–1758. https://doi.org/10.1093/brain/awn096.
Kuhlmann, T., Ludwin, S., Prat, A., Antel, J., Brück, W., Lassmann, H., 2017. An updated histological classification system for multiple sclerosis lesions. Acta Neuropathol. 133, 13–24. https://doi.org/10.1007/s00401-016-1653-y.
Locatelli, G., Theodorou, D., Kendirli, A., Jordão, M.J.C., Staszewski, O., Phulphagar, K., Cantuti-Castelvetri, L., Dagkalis, A., Bessis, A., Simons, M., Meissner, F., Prinz, M., Kerschensteiner, M., 2018. Mononuclear phagocytes locally specify and adapt their phenotype in a multiple sclerosis model. Nat. Neurosci. 21, 1196–1208. https://doi.org/10.1038/s41593-018-0212-3.
Lubetzki, C., Zalc, B., Williams, A., Stadelmann, C., Stankoff, B., 2020. Remyelination in multiple sclerosis: from basic science to clinical translation. Lancet Neurol. 19, 678–688. https://doi.org/10.1016/S1474-4422(20)30140-X.
Luchetti, S., Fransen, N.L., van Eden, C.G., Ramaglia, V., Mason, M., Huitinga, I., 2018. Progressive multiple sclerosis patients show substantial lesion activity that correlates with clinical disease severity and sex: a retrospective autopsy cohort analysis. Acta Neuropathol. 135, 511–528. https://doi.org/10.1007/s00401-018-1818-y.
Marisca, R., Hoche, T., Agirre, E., Hoodless, L.J., Barkey, W., Auer, F., Castelo-Branco, G., Czopka, T., 2020. Functionally distinct subgroups of oligodendrocyte precursor cells integrate neural activity and execute myelin formation. Nat. Neurosci. 23, 363–374. https://doi.org/10.1038/s41593-019-0581-2.
Mason, J.L., Suzuki, K., Chaplin, D.D., Matsushima, G.K., 2001. Interleukin-1β promotes repair of the CNS. J. Neurosci. 21, 7046–7052. https://doi.org/10.1523/JNEUROSCI.21-18-07046.2001.
McIntyre, L.L., Greilach, S.A., Othy, S., Sears-Kraxberger, I., Wi, B., Ayala-Angulo, J., Vu, E., Pham, Q., Silva, J., Dang, K., Rezk, F., Steward, O., Cahalan, M.D., Lane, T.E., Walsh, C.M., 2020. Regulatory T cells promote remyelination in the murine experimental autoimmune encephalomyelitis model of multiple sclerosis following human neural stem cell transplant. Neurobiol. Dis. 140, 104868. https://doi.org/10.1016/j.nbd.2020.104868.
Mei, F., Lehmann-Horn, K., Shen, Y.-A.A., Rankin, K.A., Stebbins, K.J., Lorrain, D.S., Pekarek, K., Sagan, A., Xiao, L., Teuscher, C., von Büdingen, H.-C., Wess, J., Lawrence, J.J., Green, A.J., Fancy, S.P., Zamvil, S.S., Chan, J.R., 2016. Accelerated remyelination during inflammatory demyelination prevents axonal loss and improves functional recovery. Elife 5. https://doi.org/10.7554/eLife.18246.
Melero-Jerez, C., Suardíaz, M., Lebrón-Galán, R., Marín-Bañasco, C., Oliver-Martos, B., Machín-Díaz, I., Fernández, Ó., de Castro, F., Clemente, D., 2019. The presence and suppressive activity of myeloid-derived suppressor cells are potentiated after interferon-β treatment in a murine model of multiple sclerosis. Neurobiol. Dis. 127, 13–31. https://doi.org/10.1016/j.nbd.2019.02.014.
Melero-Jerez, C., Alonso-Gómez, A., Moñivas, E., Lebrón-Galán, R., Machín-Díaz, I., de Castro, F., Clemente, D., 2020. The proportion of myeloid-derived suppressor cells in the spleen is related to the severity of the clinical course and tissue damage extent in a murine model of multiple sclerosis. Neurobiol. Dis. 140, 104869. https://doi.org/10.1016/j.nbd.2020.104869.
Melero-Jerez, C., Fernández-Gómez, B., Lebrón-Galán, R., Ortega, M.C., Sánchez-de Lara, I., Ojalvo, A.C., Clemente, D., de Castro, F., 2021. Myeloid-derived suppressor cells support remyelination in a murine model of multiple sclerosis by promoting oligodendrocyte precursor cell survival, proliferation, and differentiation. Glia 69, 905–924. https://doi.org/10.1002/glia.23936.
Mezydlo, A., Treiber, N., Ullrich Gavilanes, E.M., Eichenseer, K., Ancău, M., Wens, A., Ares Carral, C., Schifferer, M., Snaidero, N., Misgeld, T., Kerschensteiner, M., 2023. Remyelination by surviving oligodendrocytes is inefficient in the inflamed mammalian cortex. Neuron 111, 1748–1759.e8. https://doi.org/10.1016/j.neuron.2023.03.031.
Miron, V.E., Boyd, A., Zhao, J.-W., Yuen, T.J., Ruckh, J.M., Shadrach, J.L., van Wijngaarden, P., Wagers, A.J., Williams, A., Franklin, R.J.M., Ffrench-Constant, C., 2013. M2 microglia and macrophages drive oligodendrocyte differentiation during CNS remyelination. Nat. Neurosci. 16, 1211–1218. https://doi.org/10.1038/nn.3469.
Moliné-Velázquez, V., Cuervo, H., Vila-del Sol, V., Ortega, M.C., Clemente, D., de Castro, F., 2011. Myeloid-derived suppressor cells limit the inflammation by promoting T lymphocyte apoptosis in the spinal cord of a murine model of multiple sclerosis. Brain Pathol. 21, 678–691. https://doi.org/10.1111/j.1750-3639.2011.00495.x.
Moliné-Velázquez, V., Ortega, M.C., Vila del Sol, V., Melero-Jerez, C., de Castro, F., Clemente, D., 2014. The synthetic retinoid Am80 delays recovery in a model of multiple sclerosis by modulating myeloid-derived suppressor cell fate and viability. Neurobiol. Dis. 67, 149–164. https://doi.org/10.1016/j.nbd.2014.03.017.
Moyon, S., Dubessy, A.L., Aigrot, M.S., Trotter, M., Huang, J.K., Dauphinot, L., Potier, M. C., Kerninon, C., Melik Parsadaniantz, S., Franklin, R.J.M., Lubetzki, C., 2015. Demyelination causes adult CNS progenitors to revert to an immature state and express immune cues that support their migration. J. Neurosci. 35, 4–20. https://doi.org/10.1523/JNEUROSCI.0849-14.2015.
Neely, S.A., Williamson, J.M., Klingseisen, A., Zoupi, L., Early, J.J., Williams, A., Lyons, D.A., 2022. New oligodendrocytes exhibit more abundant and accurate myelin regeneration than those that survive demyelination. Nat. Neurosci. 25, 415–420. https://doi.org/10.1038/s41593-021-01009-x.
Ortega, M.C., Lebrón-Galán, R., Machín-Díaz, I., Naughton, M., Pérez-Molina, I., García-Arocha, J., Garcia-Dominguez, J.M., Goicoechea-Briceño, H., Vila-del Sol, V., Quintanero-Casero, V., García-Montero, R., Galán, V., Calahorra, L., Camacho-Toledano, C., Martínez-Ginés, M.L., Fitzgerald, D.C., Clemente, D., 2023. Central and peripheral myeloid-derived suppressor cell-like cells are closely related to the

clinical severity of multiple sclerosis. Acta Neuropathol. 146, 263–282. https://doi.org/10.1007/s00401-023-02593-x.

Schwartzbach, C.J., Grove, R.A., Brown, R., Tompson, D., Then Bergh, F., Arnold, D.L., 2017. Lesion remyelinating activity of GSK239512 versus placebo in patients with relapsing-remitting multiple sclerosis: a randomised, single-blind, phase II study. J. Neurol. 264, 304–315. https://doi.org/10.1007/s00415-016-8341-7.

Sherafat, A., Pfeiffer, F., Nishiyama, A., 2021. Shaping of regional differences in oligodendrocyte dynamics by regional heterogeneity of the Pericellular microenvironment. Front. Cell. Neurosci. 15. https://doi.org/10.3389/fncel.2021.721376.

Tepavčević, V., Kerninon, C., Aigrot, M.S., Meppiel, E., Mozafari, S., Arnould-Laurent, R., Ravassard, P., Kennedy, T.E., Nait-Oumesmar, B., Lubetzki, C., 2014. Early netrin-1 expression impairs central nervous system remyelination. Ann. Neurol. 76, 252–268. https://doi.org/10.1002/ana.24201.

Zabala, A., Vazquez-Villoldo, N., Rissiek, B., Gejo, J., Martin, A., Palomino, A., Perez-Samartín, A., Pulagam, K.R., Lukowiak, M., Capetillo-Zarate, E., Llop, J., Magnus, T., Koch-Nolte, F., Rassendren, F., Matute, C., Domercq, M., 2018. P2X4 receptor controls microglia activation and favors remyelination in autoimmune encephalitis. EMBO Mol. Med. 10. https://doi.org/10.15252/emmm.201708743.